

Ripple formation on silver after irradiation with radially polarized ultrashort-pulsed lasers

George D.Tsibidis,^{a,*} Emmanuel Stratakis,^{a,b}

^aInstitute of Electronic Structure and Laser (IESL), Foundation for Research and Technology (FORTH), N. Plastira 100, Vassilika Vouton, 70013, Heraklion, Crete, Greece

^bMaterials Science and Technology Department, University of Crete, 71003 Heraklion, Greece

Abstract. We report on the morphological effects induced by the inhomogeneous absorption of cylindrically polarized femtosecond laser irradiation of silver (Ag) in sub-ablation conditions. A theoretical prediction of the role of surface plasmon excitation in the production of self-formed periodic ripples structures is evaluated. Furthermore, a combined hydrodynamical and thermoelastic model is presented to account for the influence of temperature-related lattice movements in laser beam conditions that are sufficient to produce material melting. The ability to control the size of the morphological changes via modulating the beam polarization aims to provide a systematic methodology for controlling and optimizing the outcome of laser micro-processing.

Keywords: Laser-induced damage, laser materials modification, surface plasmons, ultrafast phenomena.

* E-mail: tsibidis@iesl.forth.gr

1 Introduction

Material processing with ultra-short pulsed lasers has received considerable attention over the past decades due to its important technological applications, in particular in industry and medicine (1-7). One type of surface modification, the so-called laser-induced periodic surface structures (LIPSS) on solids have been studied extensively for linearly polarized beams. Previous theoretical approaches or experimental observations related to the formation mechanism of these structures were performed in submelting (8) or ablation conditions (9-14). With respect to the formation of ripples, various mechanisms have been proposed to account for the formation of periodic structures: interference of the incident wave with an induced scattered wave (10, 12), or with a surface plasmon wave (SPW(15)) (11, 14, 16-19), or due to self-organisation mechanisms (20).

Cylindrical vector beams (CVB) have recently gained remarkable attention as the symmetry of the polarization enables new processing strategies (21) with applications in various fields including microscopy, lithography (22), electron acceleration (23), material processing (21, 24, 25) and optical trapping (26). The cylindrical polarization states have been the topic of numerous theoretical and experimental investigations (24, 27-30). Recently, the mechanism of LIPSS formation on transient metals (i.e. nickel) upon femtosecond irradiation with CVB was explored systematically and the differences with linearly polarized beam was highlighted. While a combination of electrodynamic (i.e. related to surface plasmon excitation) and hydrodynamic effects were proposed to explain the periodically modulated surface for nickel which is a material characterized with very strong electron-phonon coupling constant, it is equally important to investigate whether metals with relatively smaller electron-phonon ($e-ph$) coupling strength also demonstrate similarly pronounced morphologies. This is due to the fact that the magnitude of the $e-ph$ strength determines the efficiency with which inhomogeneous laser energy distribution is transferred to the electron system firstly, and lattice system secondly (through the electron-phonon interaction). Hence, larger electron-phonon strengths are expected to lead to more pronounced ripples which has been observed experimentally for linearly polarized beams for noble metals (31). Nevertheless, a more conclusive investigation requires a systematic analysis of the induced surface profile after irradiation with more complex laser beam profiles (i.e. CVB). To illustrate the impact of this type of beams, we consider irradiation of silver (Ag) with radially polarized beams of moderate fluence that is sufficient to produce material melting (where energy deposition is higher) whereas only elasto-plastic effects occur elsewhere. The aforementioned processes are described by the well-established two temperature model (TTM) (32) which sheds light on all stages characterizing laser-matter interactions: (i)

energy deposition and absorption, (ii) electron excitation, (iii) heat transfer from electrons to the lattice. The model is enriched with components that account for fluid dynamics and lattice displacements. Such a thorough investigation allows an elucidation of the fundamental mechanisms of laser-matter interactions and provides a quantitative analysis that enhances our understanding of laser damage of solids after using femtosecond pulses.

In this work, we present numerical results obtained in the modelling of femtosecond interactions with Ag after repetitive radially polarized beams. The main objective is to illustrate the predominant mechanisms that characterise ripple formation and emphasise on the role of hydrodynamics and elastic deformations with increasing number of pulses at constant fluence. To provide a complete description, all thermophysical parameters, material optical properties as well as the electron-phonon coupling constants are assumed to be temperature-dependent (33).

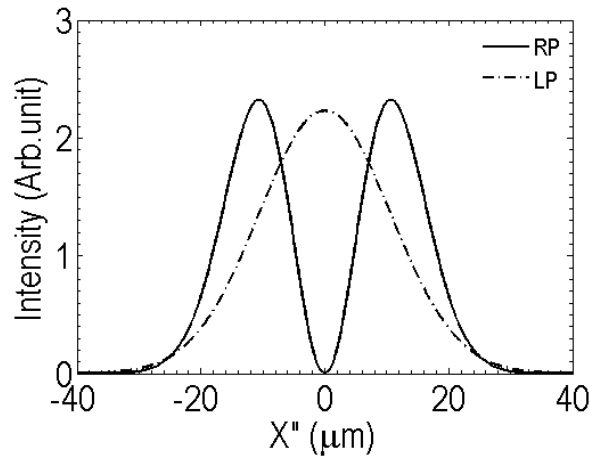


Fig. 1 Spatial intensity distribution of Radially (RP) and Linearly (LP) polarized beam. $X'' \in [-r, r]$ and it is the axis along the direction of the unit vector \hat{r} , (i.e. $\hat{r} = (\hat{x} + \hat{y})/\sqrt{2}$).

2 Theoretical Model

2.1 Polarisation of the electric field of the laser beam

We express a radially polarised beam as the superposition of orthogonally Hermite-Gauss HG_{01} and HG_{10} modes (27)

$$\vec{E}_r = HG_{10}\hat{x} + HG_{01}\hat{y} \quad (1)$$

where \vec{E}_r denotes radial polarization and \hat{x} , \hat{y} are the unit vectors along the x - and y -axis (Cartesian system), respectively (Fig.1).

2.2 Heat transfer between electron-phonon systems

The TTM constitutes the standard theoretical method to investigate laser-matter interaction which assume an instantaneous electron excitation that produces electron thermalisation (34). Although, modified versions of TTM have been also introduced to describe electron-phonon relaxation processes for very short pulses where electron thermalisation procedure is technically incorporated (35-38), the values of the pulse duration of the laser beam in the simulations (~ 170 fs) are sufficiently high to assume that the classical TTM describes efficiently electron and lattice temperature dynamics. The TTM is characterised by the following set of equations that describe energy transfer between the electron and lattice subsystems

$$\begin{aligned} C_e \frac{\partial T_e}{\partial t} &= \vec{\nabla} \cdot (\kappa_e \vec{\nabla} T_e) - g(T_e - T_L) + dI(x, y, z, t) / dz \\ C_L \frac{\partial T_L}{\partial t} &= g(T_e - T_L) \end{aligned} \quad (2)$$

where T_e and T_L are the electron and lattice temperatures, k_e and k_L stand for the electron and lattice heat conductivities, C_e and C_L correspond to the electron and lattice heat capacities, and g is the electron-

phonon coupling strength. The heat source is modelled assuming a Gaussian temporal profile and it has the following form

$$dI(x, y, z, t) / dz = -\frac{\sqrt{4 \log 2} c \varepsilon_0}{\sqrt{\pi} \tau_p} \frac{(1 - R(x, y, z = 0, t))}{1 / \alpha(x, y, z, t) + \lambda_{ball}} \exp\left(-4 \log 2 \left(\frac{t - 3\tau_p}{\tau_p}\right)^2\right) \times \frac{n(x, y, z, t)}{2} \left| \vec{E}_r(x, y, z, t) \right|^2 \exp\left(-\frac{z}{1 / \alpha(x, y, z, t) + \lambda_{ball}}\right) \quad (3)$$

where τ_p is the pulse duration, R and α stand for the reflectivity and absorption coefficient derived from the dielectric constant (39, 40), and λ_{ball} is the ballistic electron penetration depth (34, 41), c is the speed of light, ε_0 is the vacuum permittivity and n is the material refractive index. The temporal dependence of the optical parameters comes from the electron relaxation time which is the sum of the electron-electron and electron-phonon collision rates, $A(T_e)^2$ and BT_L , respectively (40). Hence, dynamic optical properties are considered in the simulations. The values of the electron conductivity k_e given by the following expression

$$k_e = \frac{\left((\theta_e)^2 + 0.16\right)^{5/4} \left((\theta_e)^2 + 0.44\right) \theta_e}{\left((\theta_e)^2 + 0.092\right)^{1/2} \left((\theta_e)^2 + \eta \theta_L\right)^{5/4}} \chi \quad (4)$$

$$\theta_e = \frac{T_e}{T_F}, \theta_L = \frac{T_L}{T_F}$$

where, in the case of silver, the parameters that appear in the expression are the Fermi temperature $T_F = 6.38 \times 10^4 \text{K}$, $\chi = 500 \text{WK}^{-1} \text{sec}^{-1}$, $\eta = 0.1715$ (36). On the other hand, the $e-ph$ coupling constant g and the electron heat capacity are evaluated through a fitting procedure based on results derived by calculating the electron density of states (DOS) (33). Finally, the lattice thermal conductivity k_L is taken as 1% of the thermal conductivity of bulk metal since the mechanism of heat conduction in metal is mainly due to electrons.

The laser conditions used in the simulations are appropriately selected to highlight the role of hydrodynamics and elasto-plastic processes and their role in surface modification. Therefore, a phase transition from solid-to-liquid has to be incorporated in the modelling framework while an investigation of lattice deformations will determine whether plastic effects can also influence the final surface profile.

2.3 Hydrodynamics

To describe the heat transfer in the molten material and fluid dynamics, it is assumed that the fluid behaves as an incompressible Newtonian fluid and its dynamics is provided by the following set of equations (to account for the mass, energy, and momentum conservation, respectively) (14)

$$\begin{aligned}\vec{\nabla} \cdot \vec{u} &= 0 \\ C_L^{(m)} \left(\frac{\partial T_L}{\partial t} + \vec{\nabla} \cdot (\vec{u} T_L) \right) - L_m \delta(T_L - T_{melt}) \frac{\partial T_L}{\partial t} &= \vec{\nabla} \cdot (\kappa_L \vec{\nabla} T_L) \\ \rho_L^{(m)} \left(\frac{\partial \vec{u}}{\partial t} + \vec{u} \cdot \vec{\nabla} \vec{u} \right) &= \vec{\nabla} \cdot \left(-P + \mu^{(m)} (\vec{\nabla} \vec{u}) + \mu^{(m)} (\vec{\nabla} \vec{u})^T \right)\end{aligned}\tag{5}$$

where \vec{u} is the fluid velocity, $\mu^{(m)}$ is the dynamic viscosity of the liquid, $\rho_L^{(m)}$ is the density of the molten material, T_{melt} is the melting temperature for Ag, L_m is the latent heat for phase transformation, P stands for pressure, k_L and $C_L^{(m)}$ stand for lattice heat conductivity and lattice heat capacity, respectively, of the molten material. The term that contains the delta function has been presented to provide a smooth transition from the solid-to liquid phase and describe efficiently the resolidification process (14).

2.4 Thermomechanical effects

To describe the thermomechanical response of the material, the following dynamic equations of elasticity are used

$$\begin{aligned}
\rho_L^{(s)} \frac{\partial^2 V_i}{\partial t^2} &= \sum_{j=1}^3 \frac{\partial \sigma_{ji}}{\partial x^j} \\
\sigma_{ij} &= 2\mu \varepsilon_{ij} + \lambda \sum_{k=1}^3 \varepsilon_{kk} \delta_{ij} - \delta_{ij} (3\lambda + 2\mu) \alpha' (T_L - T_0) \\
\varepsilon_{ij} &= 1/2 \left(\frac{\partial V_i}{\partial x^j} + \frac{\partial V_j}{\partial x^i} \right)
\end{aligned} \tag{6}$$

where σ_{ij} and ε_{ij} stand for stress and strains, while λ and μ are the Lamé's coefficients. On the other hand, V_i are the displacements along the x^i direction ($i=1,2,3$), $\rho_L^{(s)}$ is the density of (solid) Ag and α' corresponds to the thermal expansion coefficient.

Furthermore, to describe more accurately the *e-ph* relaxation process and the thermally induced strains and displacements, an additional term is incorporated in the equation that provides the lattice temperature evolution to account for the strain-related temperature variation (second equation in Eq.(7)) (8)

$$\begin{aligned}
C_e \frac{\partial T_e}{\partial t} &= \vec{\nabla} \cdot (\kappa_e \vec{\nabla} T_e) - g(T_e - T_L) + S(\vec{r}, t) \\
C_L \frac{\partial T_L}{\partial t} &= g(T_e - T_L) - (3\lambda + 2\mu) \alpha' T_L \sum_{i=1}^3 \dot{\varepsilon}_{ii}
\end{aligned} \tag{7}$$

where λ ($\equiv \frac{E\nu}{(1+\nu)(1-2\nu)}$) and μ ($\equiv \frac{E}{2(1+\nu)}$) are the Lamé's coefficients, while E and ν are the Young's modulus and Poisson ratios, respectively.

The parameters that are used in the numerical solution of the governing equations Eqs. (1-7) are listed in Table 1. A finite-difference method in a staggered grid is employed (14) to solve numerically the heat transfer equations (14), phase change (14, 15) and dynamic elasticity equations (8). Plastic effects are considered when the total stress exceeds the yield stress of the material.

Table 1 Simulation values.

Parameter	Value
E_p [J/cm ²]	0.65
λ_{photon} [nm]	800
τ_p [fs]	170
C_L [10 ⁶ Jm ⁻³ K ⁻¹]	2.50
$C_L^{(m)}$ [10 ⁶ Jm ⁻³ K ⁻¹]	(2.97-4.72×10 ⁻⁴ T_L (K ⁻¹))
A [10 ⁷ s ⁻¹ K ⁻²]	0.932
B [10 ¹¹ s ⁻¹ K ⁻¹]	1.02
T_{melt} [K]	1235
T_0 [K]	300
E [GPa]	83
ν	0.37
α' [10 ⁻⁶ K ⁻¹]	18.9
L_m [kJ/kg]	104.57
σ [N/m]	0.92
$\rho_L^{(m)}$ [Kgr/m ³]	10465-0.9067 T_L (K ⁻¹)
$\rho_L^{(s)}$ [Kgr/m ³]	10490
$\mu^{(m)}$ [mPa sec]	3.88

2.5 Surface plasmon excitation

It is known that repetitive irradiation of solids with fs pulses gives rise to excitation of SPP (11, 31). Furthermore, corrugated surfaces could also allow SPP excitation (14, 42, 43) and therefore, correlation of morphological characteristics of the irradiated zone (depth, δ and grating periodicity, A) with the magnitude of the longitudinal wavevector of the SPP requires a systematic analysis of the propagation of the respective electromagnetic field. To provide a detailed analysis of the physical mechanisms, the spatio-temporal distribution of the electric field is modelled assuming a surface profile that is determined by the approximating function (where $r=(x^2+y^2)^{1/2}$)

$$\delta(r) = D(r) \sin(2\pi r / A) \quad (8)$$

In the case of a spatially Gaussian beam, $D(r) \sim \exp(-r^2)$. By contrast, for a CVB, $D(r)$ is determined by the form of the intensity resulting from Eq.(1). The interaction between the

incident beam and the excited surface-plasmon wave is estimated assuming low modulation of the surface grating structure. Due to the axial symmetry, analysis is performed on the r - z plane, assuming a TM wave for the incident beam. The determination of the spatial distribution of the electric field and derivation of the dispersion relations comes from the solution of the Maxwell's equations by imposing the boundary condition that the tangential component of the electric field \vec{E} and normal component of $\varepsilon\vec{E}$ (ε stands for the dielectric constant of Ag) should be equal (44).

3 Results

Theoretical simulations indicate that no ripples are formed for a single pulse ($NP=1$) irradiation. In principle, surface plasmon polaritons (SPP) cannot be excited on a flat surface since the laser dispersion curve does not meet the surface plasmon dispersion curve (14, 43, 45, 46). It turns out that scattering on roughness (42) or the presence of gratings whose period is the SPP (47) allow ripple formation as the appropriate condition for surface plasmon excitation is satisfied. On the other hand, the induced surface modification after irradiation with one pulse produces a defect that allows SP excitation when the material is further irradiated (i.e. increasing NP).

To estimate the optimal laser-grating coupling, the combination of maximum depth δ and resonant length λ have been computed that yields enhanced longitudinal E_r inside the irradiation zone (44). A correlation of λ as a function of the depth is presented in Fig.2 that indicates that the resonant length is a decreasing function of the depth. Similar computations have also been performed for semiconductors (11) and for metals (44).

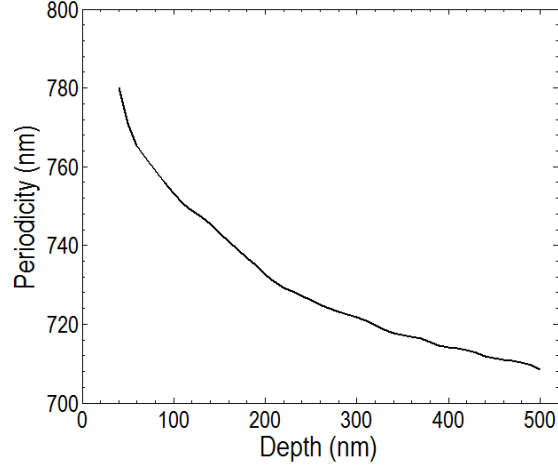


Fig. 2 Dependence of corrugation periodicity on maximum corrugation depth of modified profile ($E_p=0.65\text{J}/\text{cm}^2$, $\tau_p=170\text{fs}$).

To ensure that the laser beam conditions produce phase transitions, the maximum electron and lattice temperatures, T_e and T_L , respectively, have been plotted in Fig.3. Compared to other metals with stronger $e-ph$ coupling constant (i.e. Ti (36)), for silver, relaxation process is delayed as a result of the smaller g . The non-equilibrium between T_e and T_L illustrated in Fig.3a is explained by considering the influence of the two competing mechanisms, diffusion of electron thermal energy into deeper parts and exchange of energy between electrons and lattice. It is evident that the former mechanism dominates which is also a characteristic of metals with a relatively weak $e-ph$ coupling strength (31). The discrepancy is further enhanced by the fact there is also an increased penetration due to the inclusion of the ballistic transport of the hot electrons. Furthermore, the large value of T_e justifies the procedure followed to determine the thermophysical properties of the material and $e-ph$ coupling constant based on first-principles electronic structure calculations of the electron DOS (see (33)).

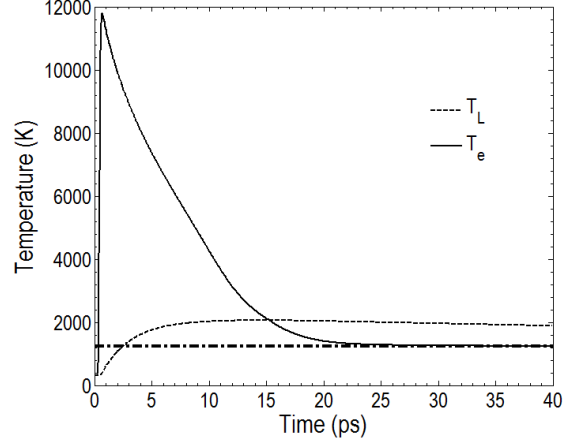


Fig. 3 Evolution of maximum electron and lattice temperatures ($E_p=0.65\text{J}/\text{cm}^2$, $NP=1$, $\tau_p=170\text{fs}$). Horizontal dash-dotted line indicates T_{melt} .

Fig.4 (a) illustrates the temperature spatial lattice temperature at $t=25\text{ps}$ (for $NP=1$) where the thermal effect of the laser beam profile is obvious. Fig. 4 (b) shows at $t=0.45\text{ns}$ the horizontal and vertical displacements where the vertical movement appears to be substantially larger. To emphasise on the fluid and elasticity related movements, focus has been restricted on the surface-tension generated movement and lattice deformations. The resolidification analysis, determined by following the evolution of the isothermal T_{melt} , allows calculation of the corrugation depth.

Similar simulations and analysis have been performed for $NP>1$. The spatial profile of the lattice temperature field as a result of the influence of ripple formation and the surface plasmon excitation is illustrated in Fig.5a for $NP=2$. The corresponding surface displacement at time $t=0.45\text{ns}$ is illustrated in Fig.5b. The theoretical calculations indicate that the produced surface profile upon resolidification is characterized not only by the formation of subwavelength ripples but also by a cone protruding along the z -axis (Fig. 5b). The emergence of a cone that has been observed experimentally in a previous work (44) is explained by the development of stress fields, rather than fluid movement, since the induced lattice temperature in the vicinity of the spot centre is not sufficient to melt the material for a CVB laser beam. In

particular, it is observed that the radius of the produced ‘Mexican-hat’ is determined by the magnitude of horizontal strain components while the peak of the cone is formed below the level of the initially flat surface (44).

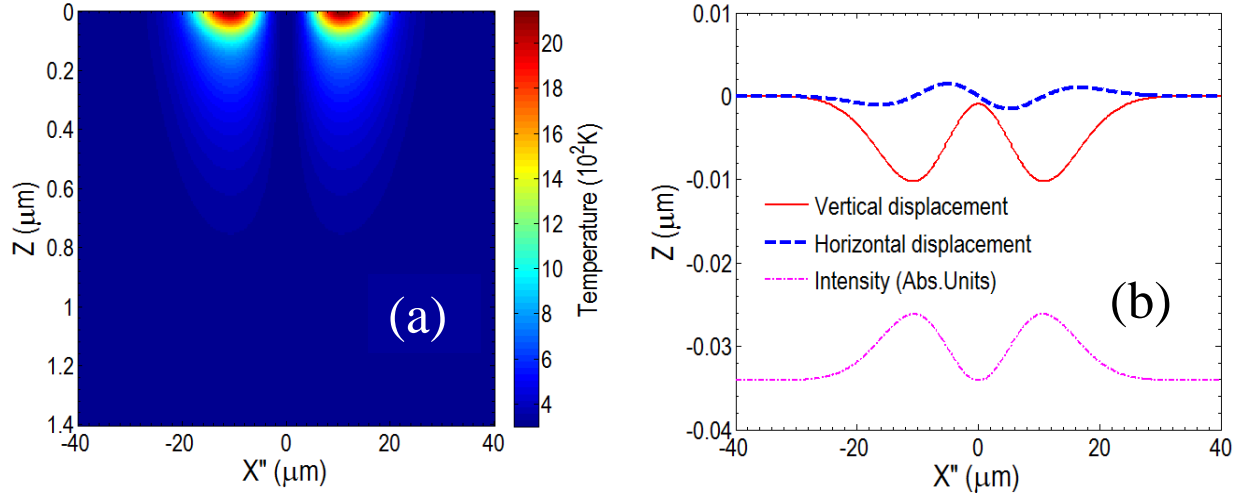


Fig. 4 (a) Lattice temperature profile at $t=25\text{ps}$, (b) Vertical and horizontal displacements at $t=0.45\text{ns}$ ($E_p=0.65\text{J}/\text{cm}^2$, $NP=1$, $\tau_p=170\text{fs}$).

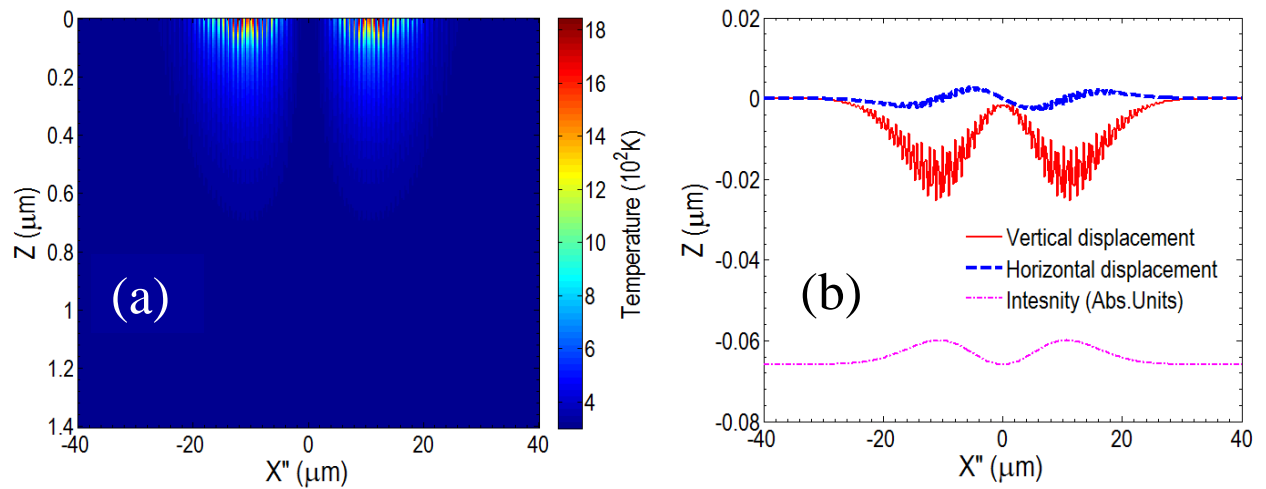


Fig. 5 (a) Lattice temperature profile at $t=25\text{ps}$, (b) Vertical and horizontal displacements at $t=0.45\text{ns}$ ($E_p=0.65\text{J}/\text{cm}^2$, $NP=2$, $\tau_p=170\text{fs}$).

In order to derive a comprehensive quantitative analysis of the morphological effects induced by radially polarized fs beams, the ripple wavelength dependence on the number of pulses has also been explored. Theoretical results illustrated in Fig.6 indicate that as the number of pulses increases, the ripple frequency increases which complies also with experimental observations for irradiation with linearly polarized beams. To emphasise on the role of hydrodynamics and elasto-pastic effects in the produced periodicity, the periodicity due to (i) only the SPP excitation and (ii) incorporation of phase transition and thermomechanical effects have been investigated. The conspicuous deviation of the wavelengths indicates the significance of the Marangoni flow and lattice movements. Thus, surface tension related forces and elastic deformations squeezes further the originally produced profile (as discussed in Section 2.5) and therefore the ripple periodicity decreases. It is important to note, though, that hydrodynamics and lattice movements do not lead to suppression of ripples. Similar behaviour has also been observed in silicon upon irradiation with femtosecond pulses (18).

The simulation results produced in this work are promising. Indeed, a first conclusion is that the model which describes energy absorption, electron excitation, heat transfer, relaxation processes enriched with a combination of phase changes and thermomechanical response of the material offers a well-defined procedure to account for material damage upon irradiation with femtosecond CVB pulses. It should be mentioned, though, that a systematic experimental validation of the numerical results is required to test the accuracy of the proposed model for irradiation of noble metals.

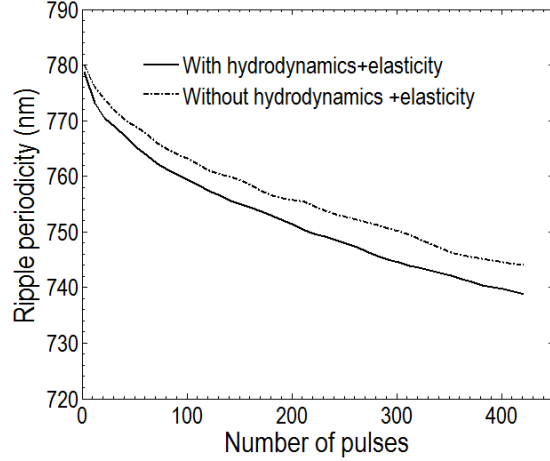


Fig. 6 Ripple periodicity dependence on number pulses ($E_p=0.65\text{J}/\text{cm}^2$, $\tau_p=170\text{fs}$). Differences in the ripple periodicity are illustrated to highlight the significance of hydrodynamics and lattice displacements.

4 Conclusions

In conclusion, we have performed numerical simulations to provide a detailed analysis of the underlying mechanisms that lead to surface modification upon irradiation of Ag with CVB fs laser pulses. The investigation shows the significant influence of the incident beam polarization on both the morphological profile as well as the size of the produced structures. Despite the emphasis on morphological effects on noble metals, the study can also be extended to other types of metals and solids, including dielectrics, semiconductors or polymers. The ability to control the size of the morphological changes via modulating the beam polarization is expected to provide novel types of surface and bulk structures with significant advantages for potential applications.

Acknowledgments

G.D.T acknowledges *LiNaBiofluid* (Grant agreement No 665337) and *Nanoscience Foundries and Fine Analysis (NFFA)–Europe* H2020-INFRAIA-2014-2015 (Grant agreement No 654360) projects for financial support.

References

1. A. Y. Vorobyev, and C. Guo, "Direct femtosecond laser surface nano/microstructuring and its applications," *Laser & Photonics Reviews* **7**(3), 385-407 (2012).
2. V. Zorba et al., "Making silicon hydrophobic: wettability control by two-lengthscale simultaneous patterning with femtosecond laser irradiation," *Nanotechnology* **17**(13), 3234-3238 (2006).
3. V. Zorba et al., "Biomimetic Artificial Surfaces Quantitatively Reproduce the Water Repellency of a Lotus Leaf," *Advanced Materials* **20**(21), 4049-+ (2008).
4. D. Bäuerle, *Laser processing and chemistry*, 3rd rev. enlarged ed., Springer, Berlin ; New York (2000).
5. J.-C. Diels, and W. Rudolph, *Ultrashort laser pulse phenomena : fundamentals, techniques, and applications on a femtosecond time scale*, 2nd ed., Elsevier / Academic Press, Amsterdam ; Boston (2006).
6. E. L. Papadopoulou et al., "Silicon Scaffolds Promoting Three-Dimensional Neuronal Web of Cytoplasmic Processes," *Tissue Eng Part C-Me* **16**(3), 497-502 (2010).
7. Z. B. Wang et al., "Femtosecond laser ablation of polytetrafluoroethylene (Teflon) in ambient air," *Journal of Applied Physics* **93**(10), 6375-6380 (2003).
8. G. D. Tsibidis, E. Stratakis, and K. E. Aifantis, "Thermoplastic deformation of silicon surfaces induced by ultrashort pulsed lasers in submelting conditions," *Journal of Applied Physics* **111**(5), 053502 (2012).
9. E. Stratakis, A. Ranella, and C. Fotakis, "Biomimetic micro/nanostructured functional surfaces for microfluidic and tissue engineering applications," *Biomicrofluidics* **5**(1), 013411 (2011).
10. J. Bonse, M. Munz, and H. Sturm, "Structure formation on the surface of indium phosphide irradiated by femtosecond laser pulses," *Journal of Applied Physics* **97**(1), 013538 (2005).
11. M. Huang et al., "Origin of Laser-Induced Near-Subwavelength Ripples: Interference between Surface Plasmons and Incident Laser," *Acs Nano* **3**(12), 4062-4070 (2009).
12. J. E. Sipe et al., "Laser-Induced Periodic Surface-Structure .1. Theory," *Physical Review B* **27**(2), 1141-1154 (1983).
13. Z. Guosheng, P. M. Fauchet, and A. E. Siegman, "Growth of Spontaneous Periodic Surface-Structures on Solids during Laser Illumination," *Physical Review B* **26**(10), 5366-5381 (1982).

14. G. D. Tsibidis et al., "Dynamics of ripple formation on silicon surfaces by ultrashort laser pulses in subablation conditions," *Physical Review B* **86**(11), 115316 (2012).
15. G. D. Tsibidis, C. Fotakis, and E. Stratakis, "From ripples to spikes: A hydrodynamical mechanism to interpret femtosecond laser-induced self-assembled structures," *Physical Review B* **92**(4), 041405(R) (2015).
16. J. Bonse, A. Rosenfeld, and J. Kruger, "On the role of surface plasmon polaritons in the formation of laser-induced periodic surface structures upon irradiation of silicon by femtosecond-laser pulses," *Journal of Applied Physics* **106**(10), 104910 (2009).
17. T. J. Y. Derrien et al., "Possible surface plasmon polariton excitation under femtosecond laser irradiation of silicon," *Journal of Applied Physics* **114**(8), 083104-083110 (2013).
18. M. Barberoglou et al., "The influence of ultra-fast temporal energy regulation on the morphology of Si surfaces through femtosecond double pulse laser irradiation," *Applied Physics A: Materials Science and Processing* **113**(273-283) (2013).
19. G. D. Tsibidis et al., "Controlled ultrashort-pulse laser-induced ripple formation on semiconductors," *Applied Physics A* **114**(1), 57-68 (2014).
20. O. Varlamova et al., "Self-organized pattern formation upon femtosecond laser ablation by circularly polarized light," *Applied Surface Science* **252**(13), 4702-4706 (2006).
21. O. J. Allegre et al., "Laser microprocessing of steel with radially and azimuthally polarized femtosecond vortex pulses," *Journal of Optics* **14**(8), 085601 (2012).
22. L. E. Helseth, "Roles of polarization, phase and amplitude in solid immersion lens systems," *Optics Communications* **191**(3-6), 161-172 (2001).
23. B. Hafizi, E. Esarey, and P. Sprangle, "Laser-driven acceleration with Bessel beams," *Physical Review E* **55**(3), 3539-3545 (1997).
24. V. G. Niziev, and A. V. Nesterov, "Influence of beam polarization on laser cutting efficiency," *Journal of Physics D-Applied Physics* **32**(13), 1455-1461 (1999).
25. R. Torres et al., "Influence of Laser Beam Polarization on Laser Micro-Machining of Molybdenum," *Journal of Laser Micro Nanoengineering* **8**(3), 188-191 (2013).
26. T. Kuga et al., "Novel optical trap of atoms with a doughnut beam," *Physical Review Letters* **78**(25), 4713-4716 (1997).
27. Q. W. Zhan, "Cylindrical vector beams: from mathematical concepts to applications," *Adv Opt Photonics* **1**(1), 1-57 (2009).
28. K. S. Youngworth, and T. G. Brown, "Focusing of high numerical aperture cylindrical-vector beams," *Optics Express* **7**(2), 77-87 (2000).
29. S. Quabis et al., "The focus of light - theoretical calculation and experimental tomographic reconstruction," *Applied Physics B-Lasers and Optics* **72**(1), 109-113 (2001).
30. M. Beresna et al., "Radially polarized optical vortex converter created by femtosecond laser nanostructuring of glass," *Applied Physics Letters* **98**(20), 201101 (2011).
31. J. Wang, and C. Guo, "Ultrafast dynamics of femtosecond laser-induced periodic surface pattern formation on metals," *Applied Physics Letters* **87**(25), 251914 (2005).
32. S. I. Anisimov, Kapeliov.BI, and T. L. Perelman, "Electron-emission from surface of metals induced by ultrashort laser pulses," *Zhurnal Eksperimentalnoi Teor. Fiz.* **66**(2), 776-781 (1974 [Sov. Phys. Tech. Phys. 11, 945 (1967)]).
33. Z. Lin, L. V. Zhigilei, and V. Celli, "Electron-phonon coupling and electron heat capacity of metals under conditions of strong electron-phonon nonequilibrium," *Physical Review B* **77**(7), 075133 (2008).

34. J. Hohlfeld et al., "Electron and lattice dynamics following optical excitation of metals," *Chemical Physics* **251**(1-3), 237-258 (2000).
35. G. D. Tsibidis, "Thermal response of double-layered metal films after ultrashort pulsed laser irradiation: The role of nonthermal electron dynamics," *Applied Physics Letters* **104**(5), 051603 (2014).
36. E. Tzianaki et al., "High acoustic strains in Si through ultrafast laser excitation of Ti thin-film transducers," *Optics Express* **23**(13), 17191-17204 (2015).
37. E. Carpene, "Ultrafast laser irradiation of metals: Beyond the two-temperature model," *Physical Review B* **74**(2), 024301 (2006).
38. M. Lisowski et al., "Ultra-fast dynamics of electron thermalization, cooling and transport effects in Ru(001)," *Applied Physics a-Materials Science & Processing* **78**(2), 165-176 (2004).
39. A. D. Rakic et al., "Optical Properties of Metallic Films for Vertical-Cavity Optoelectronic Devices," *Applied Optics* **37**(22), 5271-5283 (1998).
40. Y. P. Ren et al., "Ultrashort laser pulse energy deposition in metal films with phase changes," *Applied Physics Letters* **98**(19), 191105 (2011).
41. J. Byskov-Nielsen et al., "Ultra-short pulse laser ablation of copper, silver and tungsten: experimental data and two-temperature model simulations," *Applied Physics a-Materials Science & Processing* **103**(2), 447-453 (2011).
42. J. E. Sipe et al., "Laser-induced periodic surface structure. I. Theory," *Physical Review B* **27**(2), 1141-1154 (1983).
43. H. Raether, *Surface plasmons on smooth and rough surfaces and on gratings*, Springer-Verlag, Berlin ; New York (1988).
44. G. D. Tsibidis, E. Skoulas, and E. Stratakis, "Ripple formation on nickel irradiated with radially polarized femtosecond beams," *Optics Letters* **40**(22), 5172-5175 (2015).
45. T. J. Y. Derrien et al., "Possible surface plasmon polariton excitation under femtosecond laser irradiation of silicon," *Journal of Applied Physics* **114**(8), 083104 (2013).
46. E. Kroger, and Kretschm.E, "Scattering of Light by Slightly Rough Surfaces or Thin Films Including Plasma Resonance Emission," *Z Phys* **237**(1), 1-& (1970).
47. F. Garrelie et al., "Evidence of surface plasmon resonance in ultrafast laser-induced ripples," *Optics Express* **19**(10), 9035-9043 (2011).

Caption List

Fig. 1 Spatial intensity distribution of Radially (RP) and Linearly (LP) polarized beam. $X \in [-r, r]$ and it is the axis along the direction of the unit vector \hat{x} , (i.e. $\hat{x} = (\hat{x} + \hat{y}) / \sqrt{2}$).

Fig. 2 Dependence of corrugation periodicity on maximum corrugation depth of modified profile ($E_p=0.65\text{J}/\text{cm}^2$, $\tau_p=170\text{fs}$).

Fig. 3 Evolution of maximum electron and lattice temperatures ($E_p=0.65\text{J}/\text{cm}^2$, $NP=1$, $\tau_p=170\text{fs}$). Horizontal dash-dotted line indicates T_{melt} .

Fig. 4 (a) Lattice temperature profile at $t=25\text{ps}$, (b) Vertical and horizontal displacements at $t=0.45\text{ns}$ ($E_p=0.65\text{J}/\text{cm}^2$, $NP=1$, $\tau_p=170\text{fs}$).

Fig. 5 (a) Lattice temperature profile at $t=25\text{ps}$, (b) Vertical and horizontal displacements at $t=0.45\text{ns}$ ($E_p=0.65\text{J}/\text{cm}^2$, $NP=2$, $\tau_p=170\text{fs}$).

Fig. 6 Ripple periodicity dependence on the number pulses ($E_p=0.65\text{J}/\text{cm}^2$, $\tau_p=170\text{fs}$).

Table 1 Simulation values.



George D. Tsibidis is an Associated Researcher in the Institute of Electronic Structure and Laser at the Foundation for Research and Technology-Hellas in Heraklion, Greece. He received his PhD in theoretical particle physics from the University of Sussex, UK. His current research interests focus on the theoretical investigation of laser matter interactions for various types of materials including metals, semiconductors, and dielectrics. Particular interest is centered on material surface modification assuming electrodynamic effects, and phase transitions upon irradiation with ultrashort pulsed lasers.



Emmanuel Stratakis is a Researcher at the Institute of the Electronic Structure and Laser (IESL) of the Foundation for Research and Technology-Hellas (FORTH), where he is leading the "Ultrafast Laser Micro- and Nano- processing" activity. Dr. Emmanuel Stratakis received his PhD in 2001 from the Physics Department, University of Crete. In the fall semesters of 2006 and 2008 he was appointed as a visiting Researcher at the Department of Mechanical Engineering of the University of California, Berkeley. Since 2008 he is an Adjunct Professor at the Department of Materials Science and Technology, University of Crete. His research interests are in the fields of ultrafast laser interactions with materials for (a) biomimetic micro- and nano-structuring (b) nanomaterials synthesis, modification and functionalization for organic electronics and (c) biomaterials processing for tissue engineering.